



## Article

# The Role of GaN in the Heterostructure GaN/WS<sub>2</sub> for SERS Applications

Tsung-Shine Ko <sup>1,\*</sup> , En-Ting Lin <sup>1</sup>, Yen-Teng Ho <sup>2</sup>  and Chen-An Deng <sup>1</sup>

<sup>1</sup> Department of Electronic Engineering, National Changhua University of Education, No. 2, Shi-Da Road, Changhua 50074, Taiwan; ting19960105@gmail.com (E.-T.L.); chen880110@gmail.com (C.-A.D.)

<sup>2</sup> International College of Semiconductor Technology, National Yang Ming Chiao Tung University, Hsinchu 30010, Taiwan; chia500@nycu.edu.tw

\* Correspondence: tsko@cc.ncue.edu.tw; Tel.: +88-64-723-2105 (ext. 8367)

**Abstract:** In the application of WS<sub>2</sub> as a surface-enhanced Raman scattering (SERS) substrate, enhancing the charge transfer (CT) opportunity between WS<sub>2</sub> and analyte is an important issue for SERS efficiency. In this study, we deposited few-layer WS<sub>2</sub> (2–3 layers) on GaN and sapphire substrates with different bandgap characteristics to form heterojunctions using a chemical vapor deposition. Compared with sapphire, we found that using GaN as a substrate for WS<sub>2</sub> can effectively enhance the SERS signal, with an enhancement factor of  $6.45 \times 10^4$  and a limit of detection of  $5 \times 10^{-6}$  M for probe molecule Rhodamine 6G according to SERS measurement. Analysis of Raman, Raman mapping, atomic force microscopy, and SERS mechanism revealed that The SERS efficiency increased despite the lower quality of the WS<sub>2</sub> films on GaN compared to those on sapphire, as a result of the increased number of transition pathways present in the interface between WS<sub>2</sub> and GaN. These carrier transition pathways could increase the opportunity for CT, thus enhancing the SERS signal. The WS<sub>2</sub>/GaN heterostructure proposed in this study can serve as a reference for enhancing SERS efficiency.

**Keywords:** SERS; WS<sub>2</sub>; GaN; heterostructure; charge transfer



**Citation:** Ko, T.-S.; Lin, E.-T.; Ho, Y.-T.; Deng, C.-A. The Role of GaN in the Heterostructure GaN/WS<sub>2</sub> for SERS Applications. *Materials* **2023**, *16*, 3054. <https://doi.org/10.3390/ma16083054>

Academic Editors: Gediminas Niaura and Martynas Talaikis

Received: 10 March 2023

Revised: 7 April 2023

Accepted: 11 April 2023

Published: 12 April 2023



**Copyright:** © 2023 by the authors. Licensee MDPI, Basel, Switzerland. This article is an open access article distributed under the terms and conditions of the Creative Commons Attribution (CC BY) license (<https://creativecommons.org/licenses/by/4.0/>).

## 1. Introduction

Surface-enhanced Raman scattering (SERS) technique is a powerful tool for detecting and characterizing molecules at very low concentrations [1,2]. However, the SERS signal can still be weak for some analytes and in some experimental conditions. Improving the SERS signal would enable more sensitive detection and better characterization of molecules, which can have important applications in fields such as biomedicine, environmental monitoring, and materials science [3–6]. Additionally, a better understanding of the mechanism behind SERS enhancement is important for further optimizing the technique and developing new applications. The SERS effect is generally accepted to occur through the following two mechanisms: the electromagnetic mechanism (EM) and the chemical mechanism (CM). The use of noble metals in SERS methods is commonly adopted to achieve a significant enhancement in signal due to high electromagnetic fields around metallic structures [7,8] in the case of the EM effect. The metallic structure can provide a boost of several orders of magnitude to SERS signals. The CM effect, on the other hand, refers to the chemical interaction between the analyte molecule and the substrate [9,10]. Generally, the SERS signal of the CM effect is much lower than that of the EM effect. In recent years, several studies have demonstrated that 2D materials such as graphene, boron nitride, and molybdenum disulfide (MoS<sub>2</sub>) can be utilized as SERS substrates for biomedical detections [11,12].

Among 2D materials used for SERS measurements, tungsten disulfide (WS<sub>2</sub>) is a two-dimensional layered material that has recently attracted great interest in electronic and optoelectronic applications due to its high electron mobility, direct band gap, and strong absorption properties in the visible and near-infrared regions [13–16]. Recent

research has also pointed out that the high sensitivity, good chemical stability, and excellent biocompatibility of WS<sub>2</sub> make it highly promising for SERS applications in detecting probe molecules [17–19]. The mechanism behind the use of WS<sub>2</sub> as a SERS substrate to enhance the SERS signal intensity of the analyte is attributed to a CM, where the exciton generated under light illumination undergoes a CT process between the energy levels of the analyte and WS<sub>2</sub> at their interface, causing a significant enhancement of Raman signals achieved through charge transitions [20].

Compared to the noble metals such as Au and Ag, which are commonly used for enhancing the SERS signal through the electromagnetic mechanism, the enhancement effect of the SERS signal using CM of WS<sub>2</sub> is weaker and limited [21]. Therefore, it is necessary to enhance the signal intensity by using nanostructures. However, the process of producing nanostructured WS<sub>2</sub> is complex, and the size is difficult to control [22]. Therefore, we propose using a simple semiconductor heterostructure of WS<sub>2</sub>/GaN to effectively enhance the SERS signal. In this study, we utilized a metal-organic chemical vapor deposition (MOCVD) system to grow GaN on sapphire, followed by the deposition of a few-layer WS<sub>2</sub> film on both GaN and sapphire substrates using a furnace with chemical vapor deposition (CVD) process. After that, we compared the SERS performance of the two substrates using rhodamine (R6G) as the analyte. Our analysis, which included Raman spectroscopy, Raman mapping, atomic force microscopy (AFM), scanning electron microscopy (SEM), and X-ray photoelectron spectroscopy (XPS), showed that the quality of the WS<sub>2</sub> films grown on GaN was inferior to those grown on sapphire. Despite this, we observed that using GaN as a substrate for WS<sub>2</sub> can significantly enhance the SERS signal, with an enhancement factor of  $6.45 \times 10^4$  and a limit of detection of  $5 \times 10^{-6}$  M for the probe molecule R6G, as confirmed by SERS measurements. Through analysis of the CT mechanism, it can be inferred that an appropriate semiconductor heterostructure such as WS<sub>2</sub>/GaN can effectively provide more paths for carrier transition, making the effect of CT more intense and further enhancing the SERS signal intensity. A series of results could be expected to contribute to the development of using semiconductor heterostructures as SERS substrates.

## 2. Materials and Methods

### 2.1. Fabrication of WS<sub>2</sub>/GaN Heterostructure

A close-coupled showerhead MOCVD system was utilized to grow regular thin films of c-plane GaN on c-plane sapphire. A GaN nucleation layer with a thickness of around 30 nm was deposited by MOCVD at a growth temperature of 530 °C and a pressure of 600 mbar on c-plane sapphire substrates. The initial GaN layer was deposited at a growth temperature of 1030 °C and a pressure of 300 mbar. The temperature and pressure for the main GaN layer were set at 1050 °C and 150 mbar, respectively, with a V/III ratio of approximately 1200. The thickness of the GaN was approximately 2 µm. Afterward, the WS<sub>2</sub> film was uniformly grown on both GaN and sapphire substrates positioned at the center of the furnace through the CVD process. The Ar/H<sub>2</sub> carrier gas ratio was about 3:1 (150 sccm and 50 sccm). During growing few-layer WS<sub>2</sub>, the growth gas used was a mixture of H<sub>2</sub>S (10% to Ar) and WF<sub>6</sub>, with a flow ratio of H<sub>2</sub>S/WF<sub>6</sub> equal to 200:1.

### 2.2. Preparation of R6G Molecules

A solution of R6G (ACROS Organics, 99%, Geel, Belgium) in water with concentrations ranging from  $10^{-2}$  to  $10^{-6}$  M was prepared and dip-coated onto the WS<sub>2</sub>/GaN, WS<sub>2</sub>/sapphire, and sapphire substrates. The  $10^{-2}$  M R6G solution was also placed onto a flat sapphire as a reference substrate, thereby allowing measurement of the EF. The specimens were subjected to ambient conditions and dried on a hot plate at 70 °C for 5 min.

### 2.3. Characterizations

A confocal Raman microscopy system (Tokyo Instruments, Nanofinder 30, Tokyo, Japan) was used to perform Raman spectra and SERS analyses. The excitation was carried out by a He–Ne laser, and the laser power used was 0.1 mW for as-grown samples and

0.3 mW for the reference substrate. The laser spot size was adjusted to 3  $\mu\text{m}$  using a microscope objective with a magnification of 100 $\times$  and a numerical aperture of 0.9. The acquisition time for laser measurements was configured to 20 s, while the spectrometer employed a grating with a density of 300 lines per millimeter. The resolution of Raman spectrometer was about 0.5  $\text{cm}^{-1}$ . The spectrometer's charge-coupled device was cooled to around  $-50\text{ }^{\circ}\text{C}$ , utilizing a thermoelectric cooling chip to minimize measurement noise. Prior to measurement, the spectra were calibrated using the peak ( $520\text{ cm}^{-1}$ ) of the Si on the bulk Si substrate. The surface morphology of the samples was examined using an atomic force microscope (Veeco DI-3100, Plainview, NY, USA) through an AFM scan. SEM (FEI Helios 1200+, Hillsboro, OR, USA) revealed the morphologies and nanostructures of the as-grown samples. The chemical configurations of the samples were determined using an XPS instrument (ULVAC-PHI Phi V5000, Chigasaki, Japan) equipped with an Al K $\alpha$  X-ray source and applied to the samples for analysis.

### 3. Results and Discussion

$\text{WS}_2$  is a two-dimensional material in which the layers interact with each other through van der Waals forces [23]. Even though there is a bonding force between  $\text{WS}_2$  and the underlying GaN atoms, the resulting stress has a negligible effect on the arrangement of the lattice above  $\text{WS}_2$ . Thus, we were unable to use X-ray diffraction to analyze the aforementioned information and instead were only able to further analyze the thickness of  $\text{WS}_2$  on GaN and sapphire using Raman spectroscopy. The molecule vibration modes of the  $\text{WS}_2$  grown on GaN and sapphire substrates under identical CVD conditions were examined through Raman spectroscopy analysis. The Raman spectra depicted in Figure 1a reveal the typical  $\text{E}_{2g}^1$  and  $\text{A}_{1g}$  vibration mode peaks of  $\text{WS}_2$  for both  $\text{WS}_2/\text{GaN}$  and  $\text{WS}_2/\text{sapphire}$  samples [24], indicating successful deposition of the  $\text{WS}_2$  layer on the respective substrates. A widely recognized phenomenon in the field is that the difference in wavenumber between the two vibration modes  $\text{E}_{2g}^1$  and  $\text{A}_{1g}$  of  $\text{WS}_2$  exhibits a decreasing trend with the reduction in  $\text{WS}_2$  thickness from bulk to few-layered structures [25,26]. Based on the observed difference in wavenumber of approximately  $63\text{ cm}^{-1}$  for the  $\text{WS}_2/\text{GaN}$  sample and  $62\text{ cm}^{-1}$  for the  $\text{WS}_2/\text{sapphire}$  sample, it can be inferred that the  $\text{WS}_2$  thin film formed on both substrates has a thickness ranging from 2 to 3 layers. On the other hand, it has been reported by McCreary et al. that the quality of  $\text{WS}_2$  thin film can be determined by observing the full-width at half-maximum (FWHM) of the Raman  $\text{A}_{1g}$  peak [27]. Therefore, the  $\text{A}_{1g}$  peaks of the two samples mentioned above were fitted with Gaussian curves to obtain accurate FWHM values. As shown in Figure 1b, the FWHM of the  $\text{WS}_2\text{ A}_{1g}$  peak grown on sapphire was  $4.07\text{ cm}^{-1}$ , while that on GaN was approximately  $4.85\text{ cm}^{-1}$ . This result suggests that the  $\text{WS}_2$  grown on sapphire has better thin film quality compared to that grown on GaN. The reason for this will be discussed later.

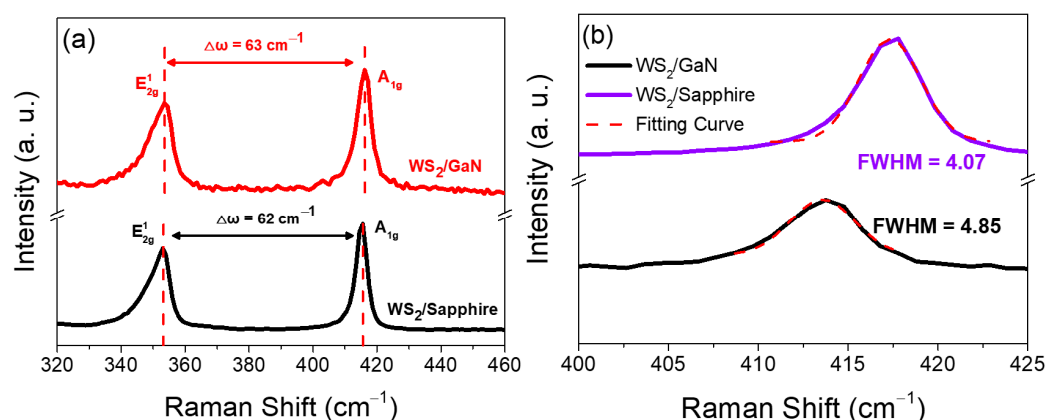


**Figure 1.** (a) Raman spectra of few-layer  $\text{WS}_2$  grown on GaN and sapphire. (b) Enlarged range of the  $\text{A}_{1g}$  peak in Figure 1a and corresponding Gaussian fitting result.

In order to further compare the uniformity of WS<sub>2</sub> grown on GaN and sapphire substrates in terms of Raman results, we further utilized Raman mapping to obtain the spatial distribution of the two peaks E<sub>2g</sub><sup>1</sup> and A<sub>1g</sub>, as well as the wavenumber difference ( $\Delta\omega$ ) between the two peaks. As shown in Figure 2, when WS<sub>2</sub> was grown on sapphire, the uniformity of both E<sub>2g</sub><sup>1</sup> and A<sub>1g</sub> peaks was significantly higher than that of GaN. In addition, the results of  $\Delta\omega$  also showed that the thickness uniformity was better when grown on sapphire. Overall, the thickness range of WS<sub>2</sub> grown on GaN was larger, which also verified the results of Figure 1a. Furthermore, our AFM measurement results, shown in Figure 3a,b, indicate that the root mean square (RMS) values of surface roughness for WS<sub>2</sub>/GaN and WS<sub>2</sub>/sapphire are 0.39 and 0.11, respectively. This suggests that the surface of WS<sub>2</sub>/GaN is rougher than that of WS<sub>2</sub>/sapphire, consistent with the aforementioned Raman and Raman mapping results. The two AFM images in Figure 3c,d provide further evidence that the surface of GaN is not as flat as that of sapphire, as the former has undergone MOCVD epitaxial growth while the latter has been polished. The RMS roughness of GaN is approximately 0.09, while that of sapphire is 0.06. We also conducted additional SEM observations, as shown in Figure S2a,b in the Supplementary Materials. The WS<sub>2</sub> grown on GaN appeared significantly rougher than the WS<sub>2</sub> grown on sapphire. It can be observed that the SEM results are consistent with the AFM results. This explains why the subsequent growth of WS<sub>2</sub> on GaN, in terms of surface uniformity and thickness uniformity, is inferior to that on sapphire. Another possible reason is that during the furnace CVD growth process, due to its higher surface activity compared to sapphire, GaN is more prone to adsorb some of the native contaminants in the furnace, such as O, C, and S atoms [28], which can affect the interface smoothness of the subsequently grown WS<sub>2</sub> film. Therefore, it can be concluded that the WS<sub>2</sub> grown on GaN exhibits inferior lattice quality and surface roughness compared to that grown on sapphire. Regarding this aspect, we provide XPS data and have a detailed discussion below.

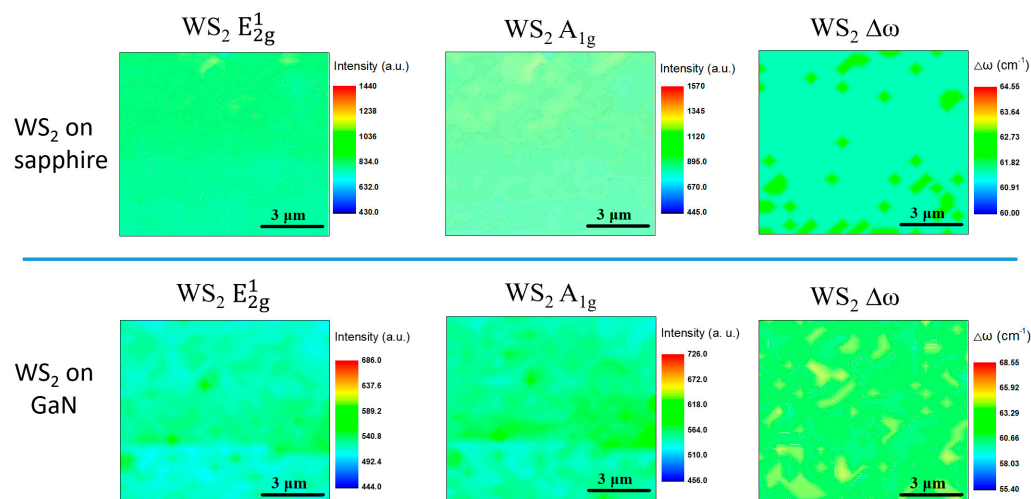


**Figure 2.** Raman mapping results of E<sub>2g</sub><sup>1</sup>, A<sub>1g</sub>, and  $\Delta\omega$  for WS<sub>2</sub>/sapphire and WS<sub>2</sub>/GaN.

To further understand the reason for the poor surface quality of WS<sub>2</sub> grown on GaN, we performed XPS experiments to analyze the content of S, C, and O atoms. The results of XPS are shown below in Figure 4a–d. Based on the signals of (a) S2p, (b) S2s, and (c) C1s, it can be concluded that when WS<sub>2</sub> was grown on GaN, both the amount of S and C atoms were higher than when it was grown on sapphire. This result is consistent with our AFM results mentioned above. Compared to sapphire, GaN is more prone to absorb S, C, and other atoms on its surface during the growth of WS<sub>2</sub>, which leads to poorer surface quality. On the other hand, as shown in Figure 4d, there are relatively more O atoms in the WS<sub>2</sub> on the sapphire structure. It is well known that sapphire has a higher affinity for oxygen compared to GaN [29]. This is because sapphire has a more polar surface with a higher surface energy, making it easier for oxygen atoms to be absorbed or captured by the surface.

In contrast, GaN has a nonpolar surface with lower surface energy, which makes it less likely for oxygen atoms to be captured or absorbed. Another possible reason for the higher concentration of O atoms could be the presence of O atoms in the sapphire substrate itself.

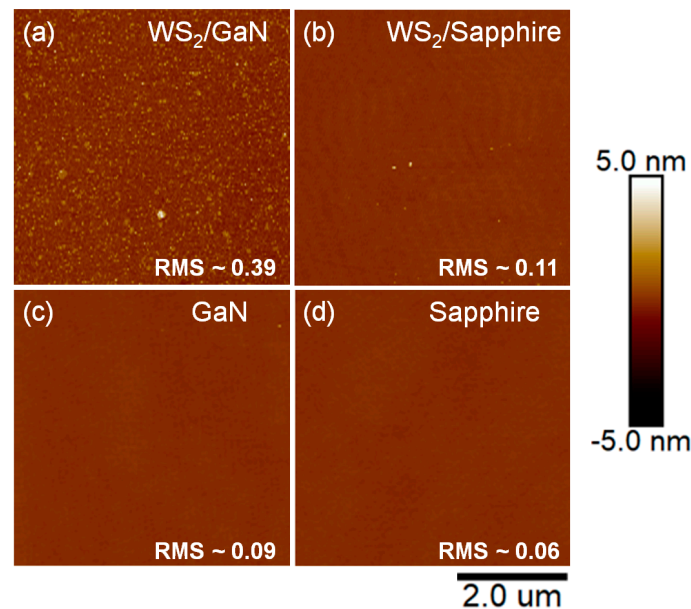


**Figure 3.** AFM images of different samples: (a)  $\text{WS}_2/\text{GaN}$ , (b)  $\text{WS}_2/\text{sapphire}$ , (c) GaN, and (d) sapphire.

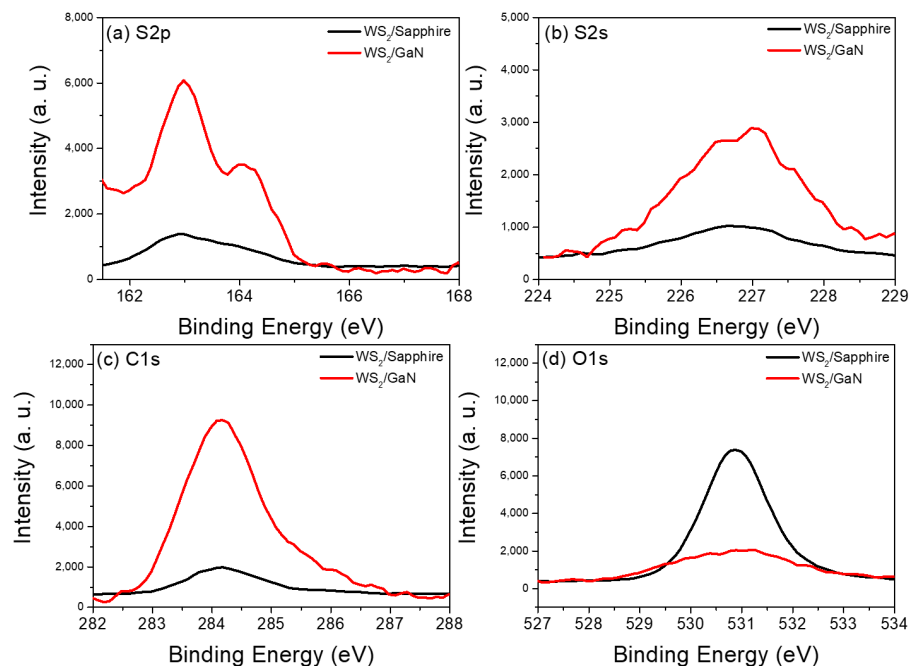


**Figure 4.** (a) S2p, (b) S2s, (c) C1s and (d) O1s core level XPS spectra of both  $\text{WS}_2/\text{GaN}$  and  $\text{WS}_2/\text{sapphire}$ .

We conducted SERS measurements on these two types of SERS substrates using R6G of  $10^{-4}$  M as the analyte, as shown in Figure 5a. The results indicate that under this range of wavenumbers, the main R6G SERS signals measured on  $\text{WS}_2/\text{GaN}$  are significantly stronger than those on  $\text{WS}_2/\text{sapphire}$ , with the peak at  $611\text{ cm}^{-1}$  being particularly prominent [30]. Although  $\text{WS}_2/\text{sapphire}$  has better film quality,  $\text{WS}_2/\text{GaN}$  shows a more prominent performance as a SERS substrate. Moreover, we used this  $\text{WS}_2/\text{GaN}$  heterostructure substrate to measure different concentrations of R6G solution, as shown in Figure 5b.



It can be observed that a weak  $611\text{ cm}^{-1}$  peak signal is still present at  $5 \times 10^{-6}\text{ M}$ , but no R6G signal can be detected at  $10^{-6}\text{ M}$ , indicating that the LOD of  $\text{WS}_2/\text{GaN}$ , in our case, can reach  $5 \times 10^{-6}\text{ M}$ . Generally, the EF is an important metric for evaluating the performance of SERS because it quantifies the level of signal enhancement that occurs when analyte molecules are adsorbed onto either a semiconductor or plasmonic substrate. EF is calculated by comparing the Raman signal intensity of a given molecule on a plasmonic substrate with that of the same molecule in its bulk form. A high EF indicates that the plasmonic substrate provides a strong enhancement effect on the Raman signal of the analyte, leading to a more sensitive detection method. Therefore, the EF value is commonly used as a figure of merit to compare the performance of different SERS substrates and to optimize the SERS experimental conditions. According to the calculation formula of EF shown in the following equation [31]:

$$\text{EF} = \frac{I_{\text{SERS}}}{I_{\text{REF}}} \times \frac{N_{\text{REF}}}{N_{\text{SERS}}}, \quad (1)$$

where  $I$  is the Raman spectral intensity and  $N$  is the number of molecules, respectively; SERS and REF denote the values obtained from  $\text{WS}_2/\text{GaN}$  and the reference sample of the sapphire substrate, respectively. As the laser spot size and exposure time were constant for all measurements, the ratio of  $N_{\text{REF}}/N_{\text{SERS}}$  was equivalent to the R6G concentration ratio for both samples. According to the above equation, it can be determined that the EF for the peak  $611\text{ cm}^{-1}$  of R6G measured using the  $\text{WS}_2/\text{GaN}$  SERS substrate can reach  $6.45 \times 10^4$ . Therefore, in terms of overall SERS performance,  $\text{WS}_2/\text{GaN}$  performs better than  $\text{WS}_2/\text{sapphire}$ . In the following discussion, we will explore the advantages of using GaN in the  $\text{WS}_2$  heterostructure for SERS measurement based on our experimental results. We also conducted measurements on the relationship between the  $611\text{ cm}^{-1}$  peak intensity and different R6G concentrations (ranging from  $10^{-4}\text{ M}$  to  $5 \times 10^{-6}\text{ M}$ ) for both samples. The results are presented in Figure S3 in the Supplementary Materials. It is apparent from the figure that the peak intensity  $\text{WS}_2/\text{GaN}$  was consistently higher than that of  $\text{WS}_2/\text{sapphire}$  in this R6G concentration range, indicating that our measurements were highly reliable.

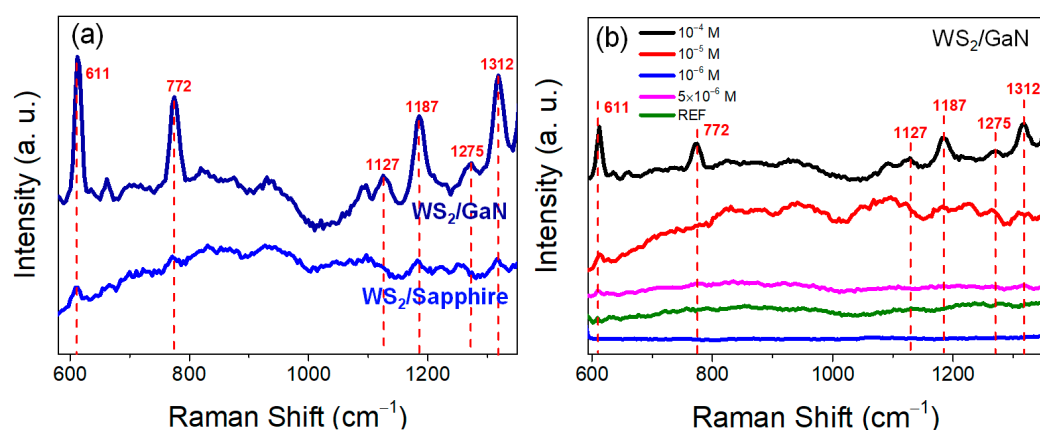


**Figure 5.** (a) Comparison of SERS results for measuring  $10^{-4}\text{ M}$  R6G using  $\text{WS}_2/\text{GaN}$  and  $\text{WS}_2/\text{sapphire}$ . (b) SERS results for different concentrations of R6G using  $\text{WS}_2/\text{GaN}$ .

In general, the enhancement mechanism of semiconductors as SERS substrates mainly comes from the CT between the photoexcited carriers and the analyte in the band gap of the semiconductor [32]. Lee et al. reported that  $\text{WS}_2$  demonstrates better SERS performance as the number of atomic layers decreases [33]. From a band perspective, our Raman results indicate that  $\text{WS}_2$  has a thickness of only about 2–3 atomic layers and a direct bandgap of about 1.6 eV [34]. The laser energy used in our experiments is approximately 1.96 eV, as shown in Figure 6, which can provide carrier transition pathways (2), (3), (5), and (6). The corresponding energy levels are the lowest unoccupied molecular orbital

(LUMO) and highest occupied molecular orbital (HOMO) of R6G, as well as the conduction band edge energy level ( $E_c$ ) and valence band edge energy level ( $E_v$ ) of  $WS_2$ . The energy differences between these pathways are all smaller than the energy of the laser, allowing  $WS_2$  to effectively enhance the SERS signal intensity of R6G. On the other hand, when GaN is introduced as a substrate for  $WS_2$  to form the  $WS_2$ /GaN heterostructure, the Raman results in Figure S1 show that the laser intensity can penetrate through the thin  $WS_2$  film and measure the oscillation frequency signals  $E_2$  and  $A_1$  of GaN [35]. This demonstrates that the laser can also excite carriers in the interface between  $WS_2$  and GaN with energy differences smaller than the laser energy. Compared to sapphire, GaN has a bandgap of approximately 3.4 eV, which at the interface with 1.6 eV of  $WS_2$ , can provide additional effective carrier transition pathways (7)–(9). This allows the excited electrons to have the opportunity to migrate to the interface between R6G and  $WS_2$ , increasing the probability of CT and enhancing the SERS signal intensity. For the purpose of comparison, we have listed the various pathways and their corresponding energy levels in Table 1, along with the possibility of carrier transition.

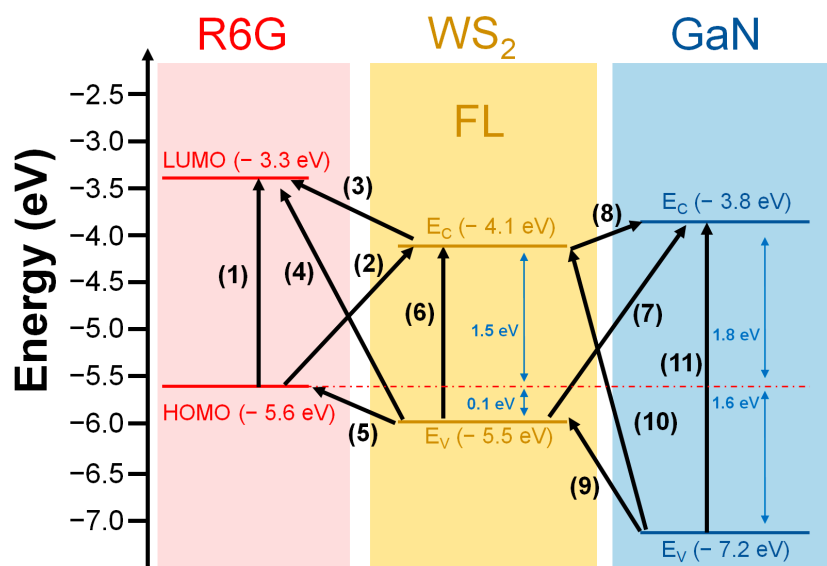


**Figure 6.** Schematic diagram of CT pathways between R6G molecules, few-layer  $WS_2$  and GaN.

**Table 1.** Corresponding energy differences and probabilities of carrier transition pathways indicated in Figure 6.

Pathways	(1)	(2)	(3)	(4)	(5)	(6)	(7)	(8)	(9)	(10)	(11)
$\Delta E$ (eV)	2.3	1.5	0.8	2.2	0.1	1.4	1.7	0.3	1.7	3.1	3.4
Possibility	X	O	O	X	O	O	O	O	O	X	X

In addition to the transition pathways between the  $WS_2$ /GaN heterostructure mentioned above that contribute to the strong SERS signal, other possibilities still need to be considered. Our AFM results show that the surface of  $WS_2$  grown on GaN is rougher than that grown on sapphire. Therefore, the higher roughness of  $WS_2$  on GaN also provides a larger contact area with the probe molecule R6G, which could enhance the SERS signal. Furthermore, in the above discussions, we mentioned that the native impurities O, C, and S in the furnace tube can be easily adsorbed onto the GaN surface, forming additional deep levels in the GaN bandgap. Therefore, these impurities may provide additional transition pathways for both  $WS_2$  and GaN, thereby increasing the SERS intensity. However, our current experimental results do not confirm the contribution of these reasons to the enhancement of the SERS signal. Therefore, in the future, we will design further experiments to analyze these possible factors.

#### 4. Conclusions

In conclusion, we propose the use of GaN as a substrate for few-layer WS<sub>2</sub> to form WS<sub>2</sub>/GaN heterostructures as SERS substrates and compare their thin film quality and SERS performance with WS<sub>2</sub>/sapphire. Through a series of experiments, including Raman, Raman mapping, AFM, and SERS mechanism investigation, our results showed that the quality of few-layer WS<sub>2</sub> film grown on GaN was inferior to that on sapphire. However, due to the high surface roughness associated with high surface contact and the additional carrier transition paths in the GaN/WS<sub>2</sub> interface, WS<sub>2</sub>/GaN heterostructures could effectively enhance SERS signals in detecting the R6G target molecule compared to WS<sub>2</sub>/sapphire, with an EF value of  $6.45 \times 10^4$  and a LOD of  $5 \times 10^{-6}$  M. Therefore, our study suggests that designing appropriate semiconductor heterostructure SERS substrates for different target molecules can effectively increase the chance of CT and enhance SERS signals.

**Supplementary Materials:** The following supporting information can be downloaded at: <https://www.mdpi.com/article/10.3390/ma16083054/s1>, Figure S1: Additional Raman results of WS<sub>2</sub>/GaN heterostructure. Figure S2: SEM images of different samples: (a) WS<sub>2</sub>/GaN, and (b) WS<sub>2</sub>/sapphire. Figure S3: A relationship between the Raman peak intensities at 611 cm<sup>-1</sup> and the R6G concentrations (from  $5 \times 10^{-6}$  to  $10^{-4}$  M).

**Author Contributions:** Conceptualization and writing—original draft preparation: T.-S.K.; methodology: E.-T.L., C.-A.D. and T.-S.K.; software: E.-T.L., C.-A.D. and T.-S.K.; validation: T.-S.K., E.-T.L. and C.-A.D.; formal analysis: T.-S.K., E.-T.L. and C.-A.D.; investigation: T.-S.K., Y.-T.H., E.-T.L. and C.-A.D.; resources: T.-S.K. and Y.-T.H.; data curation: T.-S.K. and Y.-T.H.; writing—review and editing: T.-S.K. and Y.-T.H.; visualization: T.-S.K.; supervision: T.-S.K.; project administration: T.-S.K.; funding acquisition: T.-S.K. All authors have read and agreed to the published version of the manuscript.

**Funding:** This study was funded by the National Science and Technology Council of Taiwan (grant number 1111-2221-E-018-016).

**Institutional Review Board Statement:** Not applicable.

**Informed Consent Statement:** Not applicable.

**Data Availability Statement:** Data is contained within the article or Supplementary Materials.

**Acknowledgments:** The authors thank AIXTRON (Aachen, German) for help with the deposition of the GaN thin films, Taiwan Semiconductor Research of Institute (Hsinchu, Taiwan) for the help with the measurement of XPS, Roots Technology Co., Ltd. (Hsinchu, Taiwan) for help with the deposition of the few-layer WS<sub>2</sub> and J. Shieh (National United University), as well as J.-Y. Chen (National Chung Hsing University) for assistance with Raman instrumentation and for the useful discussions.

**Conflicts of Interest:** The authors declare no conflict of interest.

#### References

1. Santhoshkumar, S.; Murugan, E. Rationally designed SERS AgNPs/GO/g-CN nanohybrids to detect methylene blue and Hg<sup>2+</sup> ions in aqueous solution. *Appl. Surf. Sci.* **2021**, *533*, 149544. [\[CrossRef\]](#)
2. Tzeng, Y.; Lin, B.-Y. Silver SERS Adenine Sensors with a Very Low Detection Limit. *Biosensors* **2020**, *10*, 53. [\[CrossRef\]](#)
3. Lai, H.; Li, G.; Xu, F.; Zhang, Z. Metal–organic frameworks: Opportunities and challenges for surface-enhanced Raman scattering—A review. *J. Mater. Chem. C* **2020**, *8*, 2952–2963. [\[CrossRef\]](#)
4. Guo, J.; Zeng, F.; Guo, J.; Ma, X. Preparation and application of microfluidic SERS substrate: Challenges and future perspectives. *J. Mater. Sci. Technol.* **2020**, *15*, 96–103. [\[CrossRef\]](#)
5. Liu, Y.; Ma, H.; Han, X.X.; Zhao, B. Metal–semiconductor heterostructures for surface-enhanced Raman scattering: Synergistic contribution of plasmons and charge transfer. *Mater. Horiz.* **2021**, *8*, 370–382. [\[CrossRef\]](#)
6. Alhmoud, H.; Brodoceanu, D.; Elnathan, R.; Kraus, T.; Voelcker, N.H. A MACEing silicon: Towards single-step etching of defined porous nanostructures for biomedicine. *Prog. Mater. Sci.* **2021**, *116*, 100636. [\[CrossRef\]](#)
7. Freeman, R.G.; Grabar, K.C.; Allison, K.J.; Bright, R.M.; Davis, J.A.; Guthrie, A.P.; Hommer, M.B.; Jackson, M.A.; Smith, P.C.; Walter, D.G.; et al. Self-Assembled Metal Colloid Monolayers: An Approach to SERS Substrates. *Science* **1995**, *267*, 1629–1632. [\[CrossRef\]](#)
8. Singh, J.P.; Chu, H.Y.; Abell, J.; Tripp, R.A.; Zhao, Y. Flexible and mechanical strain resistant large area SERS active substrates. *Nanoscale* **2012**, *4*, 3410–3414. [\[CrossRef\]](#)



9. Xia, L.; Chen, M.; Zhao, X.; Zhang, Z.; Xia, J.; Xu, H.; Sun, M. Visualized method of chemical enhancement mechanism on SERS and TERS. *J. Raman Spectrosc.* **2014**, *45*, 533–540. [\[CrossRef\]](#)
10. Chen, R.; Jensen, L. Interpreting the chemical mechanism in SERS using a Raman bond model. *J. Chem. Phys.* **2020**, *152*, 024126. [\[CrossRef\]](#)
11. Qiu, H.; Li, Z.; Gao, S.; Chen, P.; Zhang, C.; Jiang, S.; Li, H. Large-area MoS<sub>2</sub> thin layers directly synthesized on Pyramid-Si substrate for surface-enhanced Raman scattering. *RSC Adv.* **2015**, *5*, 83899–83905. [\[CrossRef\]](#)
12. Dai, Z.; Xiao, X.; Wu, W.; Zhang, Y.; Liao, L.; Guo, S.; Jiang, C. Plasmon-driven reaction controlled by the number of graphene layers and localized surface plasmon distribution during optical excitation. *Light Sci. Appl.* **2015**, *4*, e342–e348. [\[CrossRef\]](#)
13. Ernandes, C.; Khalil, L.; Almabrouk, H.; Pierucci, D.; Zheng, B.; Avila, J.; Dudin, P.; Chaste, J.; Oehler, F.; Pala, M.; et al. Indirect to direct band gap crossover in two-dimensional WS<sub>2</sub>(1–x)Se<sub>2x</sub> alloys. *NPJ 2D Mater. Appl.* **2021**, *5*, 7. [\[CrossRef\]](#)
14. Wang, Y.; Tutuc, E.; Sohler, T.; Watanabe, K.; Taniguchi, T.; Verstraete, M.J. Electron mobility in monolayer WS<sub>2</sub> encapsulated in hexagonal boron–nitride. *Appl. Phys. Lett.* **2021**, *118*, 102105. [\[CrossRef\]](#)
15. Zhang, D.; Xiong, Y.; Chai, J.; Liu, T.; Ba, X.; Cheng, J.; Ullah, S.; Zheng, G.; Yan, M.; Cao, M. Synergetic dielectric loss and magnetic loss towards superior microwave absorption through hybridization of few-layer WS<sub>2</sub> nanosheets with NiO nanoparticles. *Sci. Bull.* **2020**, *65*, 138–146. [\[CrossRef\]](#)
16. Zhang, X.; Dong, Q.; Li, Z.; Jing, X.; Liu, R.; Liu, B.; Zhao, T.; Lin, T.; Li, Q.; Liu, B. Significant pressure-induced enhancement of photoelectric properties of WS<sub>2</sub> in the near-infrared region. *Mater. Res. Lett.* **2022**, *10*, 547–555. [\[CrossRef\]](#)
17. Ghopry, S.A.; Alamri, M.A.; Goul, R.; Sakidja, R.; Wu, J.Z. Extraordinary Sensitivity of Surface-Enhanced Raman Spectroscopy of Molecules on MoS<sub>2</sub> (WS<sub>2</sub>) Nanodomes/Graphene van der Waals Heterostructure Substrates. *Adv. Optical Mater.* **2019**, *7*, 1801249. [\[CrossRef\]](#)
18. Ghopry, S.A.; Alamri, M.; Goul, R.; Cook, B.; Sadeghi, S.M.; Gutha, R.R.; Sakidja, R.; Wu, J.Z. Au Nanoparticle/WS<sub>2</sub> Nanodome/Graphene van der Waals Heterostructure Substrates for Surface-Enhanced Raman Spectroscopy. *ACS Appl. Nano Mater.* **2020**, *3*, 2354–2363. [\[CrossRef\]](#)
19. Song, Y.; Huang, H.C.; Lu, W.; Li, N.; Su, J.; Cheng, S.B.; Lai, Y.; Chen, J.; Zhan, J. Ag@WS<sub>2</sub> quantum dots for Surface Enhanced Raman Spectroscopy: Enhanced charge transfer induced highly sensitive detection of thiram from honey and beverages. *Food Chem.* **2022**, *344*, 128570. [\[CrossRef\]](#)
20. Fu, S.; Fossé, I.d.; Jia, X.; Xu, J.; Yu, X.; Zhang, H.; Zheng, W.; Krasel, S.; Chen, Z.; Wang, Z.M.; et al. Long-lived charge separation following pump–wavelength-dependent ultrafast charge transfer in graphene/WS<sub>2</sub> heterostructures. *Sci. Adv.* **2021**, *7*, eabd9061. [\[CrossRef\]](#)
21. Shin, Y.; Kim, J.; Jang, Y.; Ko, E.; Lee, N.S.; Yoon, S.; Kim, M.H. Vertically-Oriented WS<sub>2</sub> Nanosheets with a Few Layers and Its Raman Enhancements. *Nanomaterials* **2020**, *10*, 1847. [\[CrossRef\]](#)
22. Berkdemir, A.; Gutiérrez, H.R.; Botello-Méndez, A.R.; Perea-López, N.; Elías, L.A.; Chia, C.I.; Wang, B.; Crespi, V.H.; López-Urías, F.; Charlier, J.-C.; et al. Identification of individual and few layers of WS<sub>2</sub> using Raman Spectroscopy. *Sci. Rep.* **2013**, *3*, 1755. [\[CrossRef\]](#)
23. Zheng, D.; Dong, X.; Lu, J.; Niu, Y.; Wang, H. Ultrafast and hypersensitized detection based on van der Waals connection in two-dimensional WS<sub>2</sub>/Si structure. *Appl. Surf. Sci.* **2022**, *574*, 151662. [\[CrossRef\]](#)
24. Sinha, S.; Arora, S.K.; Sathe, V. Temperature Dependent Phononic Response of Liquid Phase Exfoliated Few Layered WS<sub>2</sub> Nanosheets. *AIP Conf. Proc.* **2019**, *2115*, 030197.
25. Zhang, Y.; Zhang, Y.; Ji, Q.; Ju, J.; Yuan, H.; Shi, J.; Gao, T.; Ma, D.; Liu, M.; Chen, Y.; et al. Controlled Growth of High-Quality Monolayer WS<sub>2</sub> Layers on Sapphire and Imaging Its Grain Boundary. *ACS Nano* **2013**, *7*, 8963–8971. [\[CrossRef\]](#)
26. Qiao, S.; Yang, H.; Bai, Z.; Peng, G.; Zhang, X. Thickness-dependent structural and electrical properties of WS<sub>2</sub> nanosheets obtained via the ALD-grown WO<sub>3</sub> sulfurization technique as a channel material for field-effect transistors. *ACS Omega* **2021**, *6*, 34429–34437.
27. McCreary, A.; Berkdemir, A.; Wang, J.; Nguyen, M.A.; Elías, A.L.; Perea-López, N.; Fujisawa, K.; Kabius, B.; Carozo, V.; Cullen, D.A.; et al. Distinct photoluminescence and Raman spectroscopy signatures for identifying highly crystalline WS<sub>2</sub> monolayers produced by different growth methods. *J. Mater. Res.* **2016**, *31*, 931–944. [\[CrossRef\]](#)
28. Henning, A.; Bartl, J.D.; Zeidler, A.; Qian, S.; Bienek, O.; Jiang, C.-M.; Paulus, C.; Rieger, B.; Stutzmann, M.; Sharp, I.D. Aluminum Oxide at the Monolayer Limit via Oxidant-Free Plasma-Assisted Atomic Layer Deposition on GaN. *Adv. Funct. Mater.* **2021**, *31*, 2101441. [\[CrossRef\]](#)
29. Cui, Y.; Niu, X.; Zhou, J.; Wang, Z.; Wang, R.; Zhang, J. Effect of chloride ions on the chemical mechanical planarization efficiency of sapphire substrate. *ECS J. Solid State Sci. Technol.* **2019**, *8*, 488–495. [\[CrossRef\]](#)
30. He, X.N.; Gao, Y.; Mahjouri-Samani, M.; Black, P.N.; Allen, J.; Mitchell, M.; Xiong, W.; Zhou, Y.S.; Jiang, L.; Lu, Y.F. Surface-enhanced Raman spectroscopy using gold-coated horizontally aligned carbon nanotubes. *Nanotechnology* **2012**, *23*, 205702. [\[CrossRef\]](#)
31. Chen, M.; Solarska, R.; Li, M. Additional Important Considerations in Surface-Enhanced Raman Scattering Enhancement Factor Measurements. *J. Phys. Chem. C* **2023**, *127*, 2728–2734. [\[CrossRef\]](#)
32. Lombardi, J.R.; Birke, R.L. Theory of Surface-Enhanced Raman Scattering in Semiconductors. *J. Phys. Chem. C* **2014**, *118*, 11120–11130. [\[CrossRef\]](#)

33. Lee, Y.; Kim, H.; Lee, J.; Yu, S.H.; Hwang, E.; Lee, C.; Ahn, J.-H.; Cho, J.H. Enhanced Raman Scattering of Rhodamine 6G Films on Two-Dimensional Transition Metal Dichalcogenides Correlated to Photoinduced Charge Transfer. *Chem. Mater.* **2016**, *28*, 180–187. [[CrossRef](#)]
34. Gutiérrez, H.R.; Perea-López, N.; Elías, A.L.; Berkdemir, A.; Wang, B.; Lv, R.; Lopez-Urías, F.; Crespi, V.H.; Terrones, H.; Terrones, M. Extraordinary Room-Temperature Photoluminescence in Triangular WS<sub>2</sub> Monolayers. *Nano Lett.* **2013**, *13*, 3447–3454. [[CrossRef](#)]
35. Bagnall, K.R.; Wang, E.N. Contributed Review: Experimental characterization of inverse piezoelectric strain in GaN HEMTs via micro-Raman spectroscopy. *Rev. Sci. Instrum.* **2016**, *87*, 061501. [[CrossRef](#)]

**Disclaimer/Publisher's Note:** The statements, opinions and data contained in all publications are solely those of the individual author(s) and contributor(s) and not of MDPI and/or the editor(s). MDPI and/or the editor(s) disclaim responsibility for any injury to people or property resulting from any ideas, methods, instructions or products referred to in the content.